PERGAMON

Control Engineering Practice 9 (2001) 1327–1335

CONTROL ENGINEERING PRACTICE

www.elsevier.com/locate/conengprac

H^∞ parameter identification for inflight detection of aircraft icing: the time-varying case

James W. Melody[a], Thomas Hillbrand[b], Tamer Başar[a,*], William R. Perkins[a]

[a] *Coordinated Science Laboratory, Decision and Control Laboratory, University of Illinois at Urbana-Champaign, 1308 West Main Street, Urbana, IL 61801-2307, USA*

[b] *Laboratory of Control Systems and Process Automation, Institute of Automatic Control, Darmstadt University of Technology, Landgraf-Georg-Strasse 4, D-64283 Darmstadt, Germany*

Received 2 February 2001

Abstract

This paper considers inflight parameter identification of aircraft flight dynamics in the context of an ice management system. In particular, an H^∞ parameter identification algorithm is evaluated in terms of detecting an aircraft icing event using a noisy state measurement. Previous studies had addressed identification over several seconds during a maneuver, utilizing the excitation due to the maneuver and assuming a time-invariant parameter. This paper addresses identification over longer periods, where excitation is provided only by turbulence, and parameter variation must be considered. Simulation results demonstrate that for moderate turbulence, the time-varying H^∞ algorithm provides a timely and unambiguous icing indication.

Keywords: Aircraft control; H-infinity; Identification; Time-varying systems; Robustness

1. Introduction

The past decade has exhibited increasing interest in developing aircraft that are more robust to inflight icing conditions, due in large part to the preponderance of icing as the cause of aviation accidents. For example, Cole and Sands (1991) reported that between 1975 and 1988 there were 803 known icing-related accidents in the USA, with roughly half resulting in fatalities. This interest was manifested in the national aviation safety research plan of the National Aeronautics and Space Administration (NASA) of the United States, wherein aircraft icing was determined to be a high national priority (NAS, 1997).

Aircraft icing accidents result from the effect of ice accretion on the performance, stability, and controllability of the aircraft. Small to moderate amounts of icing will generally cause a reduction in aircraft performance in terms of climb rates, range, endurance, and maximum speed and acceleration. This regime of icing effects is known as performance events. As icing increases, separation of air flow from the flight surfaces can cause loss of pilot control and even wildly unstable behavior. These more severe icing events, known as handling events, are often precipitated by a change in the aircraft configuration (e.g., flap retraction) or an aircraft maneuver effected by a pilot unaware of the flight dynamics degradation. These handling events can be classified into either tailplane stall, where the aircraft pitches forward, or asymmetric wing effects causing a roll upset. Two aspects of icing accidents are particularly of interest: (1) icing is of concern insofar as it affects the aircraft flight dynamics, and (2) icing events can be exacerbated when the pilot takes action while unaware of the severity of icing.

The new approach to aircraft icing safety, advanced by Bragg et al. (1998) and further described in some detail by Melody, Basar, Perkins, and Voulgaris (2000) is to provide the pilot with a near real-time indication of the effect of ice on the aircraft performance, stability, and controllability. Current aircraft inflight ice protection systems (IPS) consist of de-icing and anti-icing systems that respectively remove ice or inhibit accretion, as well as rudimentary stall protection systems that seek

*Corresponding author. Tel.: +1-217-333-3607; fax: +1-217-244-1653.

E-mail address: tbasar@control.csl.uiuc.edu (T. Başar).

0967-0661/01/$ - see front matter
PII: S0967-0661(01)00081-8

to restrict the aircraft to some presumed safe region of operation, or "flight envelope," by limiting pilot input. In addition to these existing ice protection systems, the proposed approach adds an ice management system (IMS) that provides three functions: (1) sensing of the presence of ice accretion and its effect on the flight dynamics; (2) activation and management of the IPS while providing the pilot with a characterization of the icing effects; and (3) modification of the flight envelope in order to maintain safe operation. As an additional level of safety, control adaptation could be added to maintain acceptable flying qualities during a performance icing event and in the worst contingency, to stabilize the aircraft after the onset of a handling event.

The IMS incorporates parameter identification of the flight dynamics, as well as external icing sensors, steady-state characterization of drag and lift using force-balance relations, and control hinge moment measurements (Bragg, 1996). Melody et al. (2001) have proposed a static feedforward neural network for synthesizing these disparate measurements into an icing characterization, building on the work of Schuchard, Melody, Başar, Perkins, and Voulgaris (2000) that applied static feedforward neural networks to flight dynamics parameter estimates only. Although all of these techniques can provide indications of the presence of icing, only parameter identification provides an explicit characterization of the type and severity of the icing effects on a parametrization of the flight dynamics, since it identifies the flight dynamics directly. In the icing context, the identification algorithms must estimate aircraft performance, stability, and control parameters over time, based on measurements of the aircraft state variables and control input. Furthermore, the algorithms must do so without the introduction of test excitation input since this input could itself induce a handling event. Excitation due to normal operational maneuvers must be sufficient. Since icing safety problems can occur at any time from takeoff to landing, effective ice detection and characterization must function in all phases of flight. Melody et al. (2000) have established the utility of H^∞ parameter identification under noisy full-state measurements during a pilot-induced longitudinal maneuver over several seconds. In this case, the parameter is essentially constant over the maneuver period, since substantial ice accretion occurs on the order of minutes. In this context, Melody et al. (2000) demonstrate that excitation due to pilot input provides parameter convergence resulting in unambiguous icing indication in a matter of seconds. The neural networks of Schuchard et al. (2000) are applied under these limited flight conditions for various icing severity levels and excitation levels, and a high degree of accuracy in both detection of tailplane icing and classification of its intensity is obtained. In this flight regime, fast icing indication is necessary in order to provide the pilot with an icing indication before the possible onset of a handling event. In the case where there is negligible excitation, steady-state characterization via force-balance equations as discussed by Bragg, Hutchison, Oltman, Pokhariyal, and Merret (2000) can be used to provide an icing indication. This paper addresses identification during steady, level flight, with moderate turbulence, filling the gap between ID during maneuver, and steady-state characterization for steady, level flight without turbulence. In this flight regime, a handling event is unlikely except in the most severe icing conditions, and hence a slower icing indication is acceptable.

2. Flight dynamics model

In actuality, all flight dynamics are nonlinear, and in this case the flight dynamics are time-varying due to the effect of ice accretion on the aerodynamics of the flight surfaces. An ideal flight dynamics model would capture both the nonlinear nature and the time variability. A typical simplification is to linearize the flight dynamics about a "trim condition" via Taylor series expansion, and to determine the values of the first-order partial derivatives via numerical simulation, wind tunnel measurements, or flight tests (Roskam, 1982). This linearization is valid for small excursions of the state from the operating condition. Since this flight dynamics model is based on the tailplane icing research of the NASA Twin Otter reported by Ratvasky, Van Zante, and Riley (1999), only the linearized longitudinal flight dynamics are considered, given by Roskam (1982) as

$$\dot{u} = -g\theta\cos(\Theta_o) + (X_u + X_{T_u})u + X_\alpha\alpha + X_{\delta_E}\delta_E, \tag{1}$$

$$\dot{w} = -g\theta\sin(\Theta_o) + Z_u u + Z_\alpha\alpha + Z_{\dot{\alpha}}\dot{\alpha} + Z_{\delta_E}\delta_E + (Z_q + U_o)q, \tag{2}$$

$$\dot{q} = (M_u + M_{T_u})u + (M_\alpha + M_{T_\alpha})\alpha + M_{\dot{\alpha}}\dot{\alpha} + M_q q + M_{\delta_E}\delta_E, \tag{3}$$

where u is the forward velocity, w is the downward velocity, q is the pitch rate, θ is the pitch angle, α is the angle of attack, and δ_E is the elevator deflection angle, the input to the system. U_o and Θ_o represent the trim values of forward velocity and pitch angle, respectively, and M_*, Z_*, and X_*, are known as "stability" or "control" derivatives, as appropriate. The effects of icing are manifested in these stability and control derivatives. During an icing encounter, the stability and control derivatives will change slowly over a period of several minutes. In particular, based on the NASA Twin Otter flight data collected in the NASA Tailplane Icing Program (TIP) and reported by Ratvasky and Ranaudo (1993), it has been determined that the only significant variations occur in the M_α, M_q, Z_α, Z_q, X_α

and $(X_u + X_{T_u})$ stability derivatives, and in the M_{δ_E} and Z_{δ_E} control derivatives. Whereas in Melody et al. (2000) these stability and control derivatives were assumed to be constant over a period of 10 s, this paper addresses identification over longer periods of time, and hence the stability and control derivatives are now allowed to be time varying.

The values for the clean and "fully" iced parameters (corresponding to a TIP simulated ice shape) are given in Table 1. These are the only two conditions for which test data exists. In order to capture a continuous variation in the stability and control derivatives, an icing severity factor $\bar{\eta}$ is used. This factor represents the degree to which the aircraft has accreted tailplane ice, with $\bar{\eta} = 0$ denoting a clean aircraft, and $\bar{\eta} = 1$ representing tailplane icing corresponding to the TIP simulated ice shape. A linear variation of the parameters with respect to this icing severity factor is assumed

$$C_* = C_*^{clean}(1 + K_{C_*}\bar{\eta}), \tag{4}$$

where C_* is any of the stability or control derivatives listed in Table 1, C_*^{clean} is its clean value, and K_{C_*} is the associated slope, determined from the parameter values corresponding to $\bar{\eta} = 1$ in Table 1. This nominal icing condition corresponds to a value of $\eta = 0.0675$ in terms of η as defined by Bragg et al. (2000).

With this model, continuous accretion of ice over time is captured by allowing $\bar{\eta}$ to vary with time. Since the ice accretion rate is a function of both atmospheric conditions and the amount of ice already accreted, and furthermore since no ice accretes without proper atmospheric conditions, the differential equation

$$\dot{\bar{\eta}} = \aleph_1(1 + \aleph_2\bar{\eta})d_\eta \tag{5}$$

is used as a model for ice accretion, where d_η represents the conduciveness of the atmosphere to icing. Although on-board test instruments exist that measure d_η in some rough sense, these instruments are not generally available, hence in this study it is assumed that d_η is unknown. The constants $\aleph_1$ and $\aleph_2$ depend in a complicated fashion on the ice collection efficiency and aerodynamics of the flight surfaces as well as on the physics of ice accretion. The values of $\aleph_1$ and $\aleph_2$ are determined from an assumed icing severity profile characterized by the duration of the icing encounter, denoted by T_{cld}, and the final and middle values of the icing severity factor, $\bar{\eta}(T_{cld})$ and $\bar{\eta}(T_{cld}/2)$, respectively. (5) is a nonlinear integrator, where $\aleph_2$ represents the degree of the nonlinearity. $\aleph_2 > 0$ results in increased ice accretion rate as ice accretion increases, and $\aleph_2 < 0$ provides the reverse. Consistent with ice accretion physics, the system is driftless in the sense that the state is fixed when the input is zero. Furthermore, this simplified model precludes discontinuities in the icing severity, as produced for example by ice shedding due to activation of the IPS.

The scenario modeled is a period of steady, level flight with turbulence through a "cloud" of icing conditions. The icing encounter is specified by its duration T_{cld} and the icing severity values at T_{cld} and at $T_{cld}/2$. In the following simulations, d_η is assumed to be a raised cosine

$$d_\eta(t) = \tfrac{1}{2}(1 - \cos(2\pi t/T_{cld})).$$

For this shape, the constants $\aleph_1$ and $\aleph_2$ in (5) as functions of the assumed values of T_{cld}, $\bar{\eta}(T_{cld})$ and $\bar{\eta}(T_{cld}/2)$ are determined via integration, which yields the relations

$$\aleph_1 = \frac{2}{\aleph_2 T_{cld}}\log[1 + \aleph_2\bar{\eta}(T_{cld})], \tag{6}$$

$$\aleph_2 = \frac{\bar{\eta}(T_{cld}) - 2\bar{\eta}(T_{cld}/2)}{\bar{\eta}^2(T_{cld}/2)}. \tag{7}$$

Two icing encounter scenarios, depicted in Fig. 1, will be investigated. The first is a moderate icing encounter that has $T_{cld} = 600$ s, $\bar{\eta}(T_{cld}) = 1$, and $\bar{\eta}(T_{cld}/2) = 0.5$. The second is a rapid and severe icing encounter that is characterized by $T_{cld} = 300$ s, $\bar{\eta}(T_{cld}) = 1.5$, and $\bar{\eta}(T_{cld}/2) = 1$. For each scenario, the parameter estimates are evaluated in terms of reliability and timeliness. By reliable, it is meant that the parameter estimates for clean and iced aircraft are distinguishable. Hence both clean and icing scenarios will be considered. Timeliness means roughly that the pilot should have an unambiguous indication of at least some level of icing before the icing severity becomes critical. This timeliness is measured in terms of the delay between the time when $\bar{\eta}$ obtains some level, and the time when the estimate of $\bar{\eta}$ reaches that level.

Table 1
Values of stability and control derivatives of the NASA Twin Otter that are affected by icing. These derivatives constitute the parameter vector χ in (8). Values are given for both the clean and nominally iced ($\bar{\eta} = 1$) conditions

	M_α	M_{δ_E}	M_q	Z_α	Z_{δ_E}	Z_q	X_α	$X_u + X_{T_u}$
Clean	−7.86	−10.44	−3.055	−378.7	−40.30	−19.70	13.71	−0.018
Nominally Iced	−7.08	−9.40	−2.948	−342.7	−36.45	−19.43	13.90	−0.020

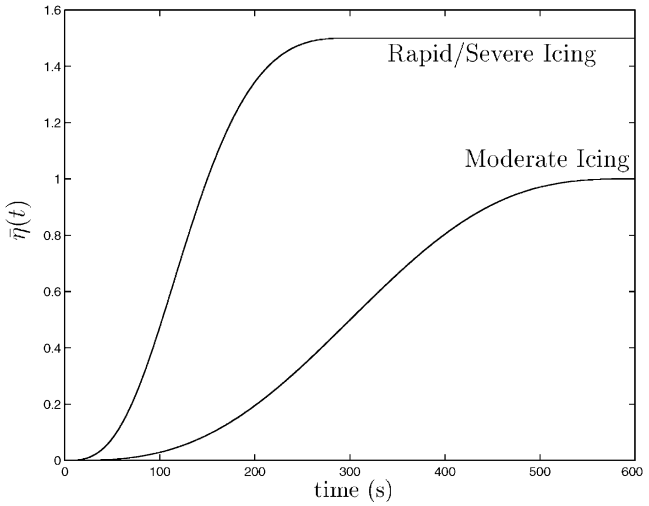

Fig. 1. Icing severity factor, $\bar{\eta}(t)$, for moderate and severe icing scenarios.

3. H^∞ parameter ID algorithm

In Melody et al. (2000) the linearized flight dynamics model has been converted into the general parameter identification framework considered by Didinsky, Pan, and Başar (1995) for time-invariant parameter systems

$$\dot{x} = A(x,v)\chi + b(x,v) + d_p, \tag{8}$$

$$y = x + d_m \tag{9}$$

via the assignments $x = \mathrm{col}(q, \theta, \alpha, u)$, $\chi = \mathrm{col}(M_\alpha, M_{\delta_E}, M_q, Z_\alpha, Z_{\delta_E}, Z_q, X_\alpha, X_u + X_{T_u})$, and $v = \delta_E$. Here $x \in \mathbb{R}^n$ is the system state, $y \in \mathbb{R}^n$ is the measured output, $v \in \mathbb{R}^m$ is the input, $d_p \in \mathbb{R}^n$ is the (unknown) process disturbance, $d_m \in \mathbb{R}^n$ is the measurement noise, and $\chi \in \mathbb{R}^r$ is the parameter vector to be estimated. In the case of systems with time-varying parameters, the formulation incorporates a linear model of the parameter evolution

$$\dot{\chi} = H\chi + Kd_\chi, \quad \chi(0) = \chi_o, \tag{10}$$

where $d_\chi \in \mathbb{R}^s$ is unknown and represents uncertainty in the parameters. Note that A, b, H, and K in general may depend explicitly upon time, although this dependence will be suppressed in the notation. The goal is to obtain estimates of the parameters from the available information, that will be accurate in the presence of disturbances and measurement noise.

As reported by Melody et al. (2000), it has been determined that only the pitching moment derivatives M_α, M_{δ_E}, and M_q provide useful estimates. The Z parameters generally converge too slowly, and the X parameters are too sensitive to noise. During steady-level flight, the M_{δ_E} parameter cannot be identified, since it is the coefficient of the input $\delta_E \equiv 0$. Furthermore, although the M_q estimate is useful for icing detection in the absence of measurement noise, it is not useful when measurement noise is added. Hence only the M_α estimate will be used for icing detection in the forthcoming simulations.

In order to obtain (10) to be used by the ID algorithm for the icing problem, a linearization of (5) is performed with the composition of the Eq. (4) as an output equation about the expected operating condition, $\bar{\eta} = 0$ and $d_\eta = 0$. Since the system is driftless, $H = 0$, and thus $K = \aleph_1\aleph_2[K_*]$, where $[K_*]$ is a vector whose elements are K_* and again $*$ varies over the stability and control derivatives in Table 1. Of course, the actual values of $\aleph_1$ and $\aleph_2$ will not be known a priori, since they are in turn dependent upon the characteristics of the icing encounter according to (6) and (7). Hence for the identification algorithm, a value of K will be used that corresponds to the values of $\aleph_1$ and $\aleph_2$ for the moderate icing encounter.

The H^∞ approach to identification treats noise signals as deterministic but unknown quantities. For the icing identification problem, it is assumed that only noisy measurements of the state are available. Didinsky et al. (1995) develop an H^∞ identification algorithm for this information state, known as the noise-perturbed full-state information (NPFSI) case, and for systems of the form

$$\dot{x} = A(y,v)\chi + b(y,v) + d_p, \tag{11}$$

$$y = x + d_m. \tag{12}$$

Note that this system differs from (8) and (9) in that $A(\cdot\,, u)$ and $b(\cdot\,, u)$ have y as an argument. This problem formulation allows Didinsky et al. (1995) to treat the identification problem as a linear H^∞ state estimation problem, resulting in an ID algorithm for (10)–(12) which seeks to achieve a guaranteed disturbance attenuation level γ between the unknown quantities and the parameter estimate error of the form

$$\|\chi - \hat{\chi}\|^2_{Q(y,v)} \leqslant \gamma^2(\|d_p\|^2 + \|d_m\|^2 + \|d_\chi\|^2 + |\chi_o - \hat{\chi}_o|^2_{Q_o} + |x_o - \hat{x}_o|^2_{P_o}) \tag{13}$$

for all $\chi_o \in \mathbb{R}^r$, $x_o \in \mathbb{R}^n$, and $d_p, d_m, d_\chi \in L_\infty \cap L_2$ where $\hat{\chi}_o$ is an a priori estimate of the parameter vector χ, $\|\cdot\|_Q$ is an L_2 norm with a chosen weighting function $Q(y,v) \geqslant 0$, $|\cdot|_{Q_o}$ is a generalized Euclidean norm with a chosen weighting matrix $Q_o > 0$, and similarly $P_o > 0$ is a chosen weighting matrix. Didinsky et al. (1995) address this problem by defining a (problem dependent) best-achievable disturbance attenuation level γ^* with the property that for any $\gamma > \gamma^*$, (13) is achieved for all $(d_p, d_m, d_\chi, \chi_o, x_o)$. In general, γ^* is not known, and it may even be infinite (meaning that no guaranteed disturbance attenuation level can be achieved). Here it will be shown that γ^* is finite for a particular choice of the weighting matrix Q.

The NPFSI algorithm for the time-varying system (8)–(10) is described for $\gamma \geqslant \gamma^*$ by

$$\begin{bmatrix} \dot{\hat{x}} \\ \dot{\hat{\chi}} \end{bmatrix} = \begin{bmatrix} 0 & A(y,v) \\ 0 & H \end{bmatrix} \begin{bmatrix} \hat{x} \\ \hat{\chi} \end{bmatrix} + \begin{bmatrix} b \\ 0 \end{bmatrix} + \Sigma^{-1} \begin{bmatrix} I \\ 0 \end{bmatrix} (y - \hat{x}), \tag{14}$$

$$\dot{\Sigma} = -\Sigma \begin{bmatrix} 0 & A(y,v) \\ 0 & H \end{bmatrix} - \begin{bmatrix} 0 & 0 \\ A(y,v)^{\mathrm{T}} & H^{\mathrm{T}} \end{bmatrix} \Sigma + \begin{bmatrix} I & 0 \\ 0 & -\gamma^{-2} Q(y,v) \end{bmatrix} - \Sigma \begin{bmatrix} I & 0 \\ 0 & KK^{\mathrm{T}} \end{bmatrix} \Sigma \tag{15}$$

with initial conditions $\hat{\chi}(0) = \hat{\chi}_o$ and $\Sigma(0) = \mathrm{diag}(P_o, Q_o)$, and where $\hat{\chi}(t)$ is the estimate of parameter $\chi(t)$ and $\Sigma(t) \in \mathbb{R}^{(n+r)\times(n+r)}$. (The NPFSI identification algorithm used by Melody et al. (2000) for the constant-parameter case ($\dot{\chi} = 0$) is recovered from (14) and (15) by setting $H = 0$ and $K = 0$.) Design of the algorithm in (14) and (15) entails the choices of the cost terms $Q(y, v)$, Q_o, and P_o, as well as the choice of some $\gamma > \gamma^*$. In fact, Q is allowed to be a function of not only the current value of y, but also its past values. Typically, Q is chosen so that γ^*, or at least some upper bound on γ^*, can be determined analytically. To arrive at a choice of Q which yields a known γ^*, the result of Didinsky et al. (1995) is used which states that for a given γ, if $\Sigma(t) > 0$ for all possible v, d_p, d_m, d_χ, $\hat{x}_o$, and $\hat{\chi}_o$, then $\gamma^* \leqslant \gamma$. Conversely, if for a particular γ, there is some time t_1 and some $(v, d_p, d_m, d_\chi, \hat{x}_o, \hat{\chi}_o)$ for which $\Sigma(t_1) \not\geqslant 0$, then $\gamma^* > \gamma$.

This result can be used to specify an NPFSI algorithm with $\gamma^* \leqslant 1$. Using the partition

$$\Sigma =: \begin{bmatrix} \Sigma_1 & \Sigma_2 \\ \Sigma_2^{\mathrm{T}} & \Sigma_3 \end{bmatrix}$$

with $\Sigma_1 \in \mathbb{R}^{n\times n}$, the Schur test for positivity states that $\Sigma(t) > 0$ if and only if $\Sigma_1(t) > 0$ and $\Pi(t) > 0$ where $\Pi := \Sigma_3 - \Sigma_2^{\mathrm{T}} \Sigma_1^{-1} \Sigma_2$. Following an argument similar to that of Didinsky et al. (1995), from (15) it can be shown that

$$\dot{\Sigma}_1 = I - \Sigma_1 \Sigma_1 - \Sigma_2 KK^{\mathrm{T}} \Sigma_2^{\mathrm{T}}, \quad \Sigma_1(0) = P_o, \tag{16}$$

$$\dot{\Sigma}_2 = -\Sigma_1 A - \Sigma_2 H - \Sigma_1 \Sigma_2 - \Sigma_2 KK^{\mathrm{T}} \Sigma_3, \quad \Sigma_2(0) = 0, \tag{17}$$

$$\dot{\Sigma}_3 = -\Sigma_2^{\mathrm{T}} A - A^{\mathrm{T}} \Sigma_2 - \Sigma_3 H - H^{\mathrm{T}} \Sigma_3 - \Sigma_2^{\mathrm{T}} \Sigma_2 - \Sigma_3 KK^{\mathrm{T}} \Sigma_3 - \gamma^{-2} Q, \quad \Sigma_3(0) = Q_o \tag{18}$$

and after some manipulation

$$\dot{\Pi} = -\Pi H - H^{\mathrm{T}} \Pi - \Pi KK^{\mathrm{T}} \Pi + \Sigma_2^{\mathrm{T}} \Sigma_1^{-2} \Sigma_2 - \gamma^{-2} Q, \quad \Pi(0) = Q_o. \tag{19}$$

Choosing $Q = \Sigma_2^{\mathrm{T}} \Sigma_1^{-2} \Sigma_2 \geqslant 0$ and $\gamma = 1$, (19) becomes

$$\dot{\Pi} = -\Pi H - H^{\mathrm{T}} \Pi - \Pi KK^{\mathrm{T}} \Pi. \tag{20}$$

It is well known that the solution to (20) with $\Pi(0) = Q_o > 0$ is positive definite for all $t < \infty$ so long as H, which is allowed to be time-varying, is uniformly bounded in time. (That this is true is easily obtained by noticing that $S(t) := \Pi^{-1}(t)$ is the solution to the differential equation $\dot{S} = KK^{\mathrm{T}} + HS + SH^{\mathrm{T}}$, with $S(0) = Q_o^{-1}$ and additionally that the solution exists for all finite positive time.)

Furthermore, for any $\gamma > 1$, and assuming for the moment that $\Sigma_1 \geqslant 0$

$$\begin{aligned} \dot{\Pi} &= -\Pi H - H^{\mathrm{T}} \Pi - \Pi KK^{\mathrm{T}} \Pi + (1 - \gamma^{-2}) \Sigma_2^{\mathrm{T}} \Sigma_1^{-2} \Sigma_2 \\ &\geqslant -\Pi H - H^{\mathrm{T}} \Pi - \Pi KK^{\mathrm{T}} \Pi \end{aligned}$$

and $\Pi(t)$ is again positive definite for all positive time. Hence, $\gamma^* \leqslant 1$ so long as $\Sigma_1(t) > 0$ for $\gamma \geqslant 1$ and for all finite time. Using $\Omega_1(t) := \Sigma_1^{-1}(t)$ it is clear that $\Sigma_1(t) > 0$ so long as $\Omega_1(t)$ remains finite. From (16)

$$\dot{\Omega}_1 = I - \Omega_1 \Omega_1 + \Omega_1 \Sigma_2 KK^{\mathrm{T}} \Sigma_2^{\mathrm{T}} \Omega_1 \tag{21}$$

with $\Omega_1(0) = P_o^{-1} > 0$. Finiteness of the solution to (21) for any finite time $T > 0$ is demonstrated by showing that the last term is bounded by $\kappa\Omega_1$ for some $\kappa \in \mathbb{R}$. In order to see this, first notice that

$$\Omega_1 \Sigma_2 KK^{\mathrm{T}} \Sigma_2^{\mathrm{T}} \Omega_1 \leqslant \rho(KK^{\mathrm{T}}) \Omega_1 \Sigma_2 \Sigma_2^{\mathrm{T}} \Omega_1, \tag{22}$$

where $\rho(\cdot)$ denotes the spectral radius. Furthermore, using the unique positive definite Cholesky decomposition of Ω_1, denoted $\Omega_1^{1/2}$,

$$\begin{aligned} \Omega_1 \Sigma_2 \Sigma_2^{\mathrm{T}} \Omega_1 &= \Omega_1^{1/2} \Omega_1^{1/2} \Sigma_2 \Sigma_2^{\mathrm{T}} \Omega_1^{1/2} \Omega_1^{1/2} \\ &\leqslant \rho(\Omega_1^{1/2} \Sigma_2 \Sigma_2^{\mathrm{T}} \Omega_1^{1/2}) \Omega_1 \\ &= \rho(\Sigma_2^{\mathrm{T}} \Omega_1 \Sigma_2) \Omega_1. \end{aligned}$$

Substituting back into (21) yields

$$\begin{aligned} \dot{\Omega}_1 &\leqslant I - \Omega_1 \Omega_1 + \rho(KK^{\mathrm{T}}) \rho(\Sigma_2^{\mathrm{T}} \Sigma_1^{-1} \Sigma_2) \Omega_1 \\ &= I - \Omega_1 \Omega_1 + \rho(KK^{\mathrm{T}}) \rho(\Sigma_3 - \Pi) \Omega_1 \\ &\leqslant I - \Omega_1 \Omega_1 + \rho(KK^{\mathrm{T}}) \rho(\Sigma_3) \Omega_1. \end{aligned}$$

If $\rho(\Sigma_3(t))$ is bounded on $[0, T]$, then the comparison lemma (Khalil, 1996) demonstrates that Ω_1 is also bounded on $[0, T]$. Keeping in mind the evolution of $\Sigma_3(t)$ for $Q := \Sigma_2^{\mathrm{T}} \Sigma_1^{-2} \Sigma_2$ and $\gamma = 1$,

$$\dot{\Sigma}_3 = -\Sigma_2^{\mathrm{T}} A - A^{\mathrm{T}} \Sigma_2 - \Sigma_3 H - H^{\mathrm{T}} \Sigma_3 - \Sigma_2^{\mathrm{T}} \Sigma_2 - \Sigma_3 KK^{\mathrm{T}} \Sigma_3 - \Sigma_2^{\mathrm{T}} \Sigma_1^{-2} \Sigma_2,$$

rearrangement of $(\Sigma_2 + A(t))^{\mathrm{T}} (\Sigma_2 + A(t)) \geqslant 0$ yields

$$-\Sigma_2^{\mathrm{T}} \Sigma_2 - A(t)^{\mathrm{T}} \Sigma_2 - \Sigma_2^{\mathrm{T}} A(t) \leqslant A(t)^{\mathrm{T}} A(t).$$

Furthermore, assuming that $A(t)$ is piecewise continuous (and hence that the control input $v(t)$ is piecewise continuous as well), there exists some matrix $M > 0$ with $A(t)^{\mathrm{T}} A(t) \leqslant M$ for all $t \in [0, T]$. With this consideration, it is easily shown that for all $\gamma \geqslant 1$

$$\dot{\Sigma}_3 \leqslant M - \Sigma_3 H - H^{\mathrm{T}} \Sigma_3 - \Sigma_3 KK^{\mathrm{T}} \Sigma_3 - \Sigma_2^{\mathrm{T}} \Sigma_1^{-2} \Sigma_2. \tag{23}$$

This shows that although Σ_3 may increase without bound as $t \to \infty$, it will always be bounded on any finite interval $[0, T]$, i.e., it will not exhibit finite escape. Thus $\Sigma_1(t) \geqslant 0$ for all $t < \infty$ and $\gamma^* \leqslant 1$ is established. In fact, slight modification of the above argument demonstrates that $\gamma^* = 1$ in general.

Thus for any $\gamma > 1$, the disturbance attenuation ratio in (13) is guaranteed to hold for the system in (10)–(12). However, the icing problem has the form (8)–(10). Fortunately, if the ID algorithm of (14) and (15) is applied to the icing problem, a disturbance attenuation level of sorts can be achieved. To see this, first recall from Melody et al. (2000) that $A(x, u)$ and $b(x, u)$ due to the linearity of the flight dynamics model have the form

$$A(x, v) = [A_1 x + B_1 v \cdots A_r x + B_r v], \tag{24}$$

$$b(x, v) = A_o x + B_o v \tag{25}$$

for some A_i, B_i, $i \in \{0, \ldots, r\}$, of appropriate dimension where r is the dimension of χ. This enables the following modification to (8) and (9)

$$\dot{x} = A(y, v)\chi + b(y, v) + d_p - A(d_m, 0)\chi - b(d_m, 0),$$

$$y = x + v.$$

With the definition $\tilde{d}_p := d_p - A(d_m, v)\chi - b(d_m, v)$, the icing problem is transformed into the NPFSI problem of Didinsky et al. (1995) in (11) and (12) with process disturbance $\tilde{d}_p$. Thus for any $\gamma > \gamma^*$

$$\begin{aligned} \|\chi - \hat{\chi}\|^2_{Q(y,v)} \leqslant \gamma^2 (&\|\tilde{d}_p\|^2 + \|d_m\|^2 + \|d_\chi\|^2 \\ &+ |\chi_o - \hat{\chi}_o|^2_{Q_o} + |x_o - \hat{x}_o|^2_{P_o}) \end{aligned} \tag{26}$$

for all $\chi_o \in \mathbb{R}^r$, $x_o \in \mathbb{R}^n$, and $\tilde{d}_p, d_m, d_\chi \in L_\infty \cap L_2$. From (24) and (25) it is clear that $\tilde{d}_p \in L_\infty \cap L_2$ whenever $d_p, v \in L_\infty \cap L_2$ if χ is well-behaved (e.g., uniformly bounded in time).

The question is whether (26) provides useful disturbance attenuation for the original problem, in the sense that the parameter estimate error norm grows in a well-behaved fashion as the unknown signal norms grow large and furthermore that the weighted error norm vanishes as the unknowns vanish. Addressing this question begins with making the definition $F(\chi) := \sum_{i=1}^{r} A_i \chi_i + A_o$ where χ_i is the ith element of χ. Then

$$A(d_m, 0)\chi + b(d_m, 0) = F(\chi) d_m.$$

Concentrating on the $\tilde{d}_p$ term of (26) provides

$$\|\tilde{d}_p\|^2 \leqslant 2\|d_p\|^2 + 2\|F(\chi) d_m\|^2.$$

Furthermore, if it is assumed that there exists a bound $|\chi(t)| \leqslant \bar{\chi}$ for all time t, as there does in the icing case, then

$$\|F(\chi) d_m\|^2 \leqslant (1 + \bar{\chi}^2) \int_0^\infty |[A_o d_m(t) \cdots A_r d_m(t)]|^2 \, \mathrm{d}t,$$

where the norm under the integral is an induced Euclidean matrix norm. Furthermore, using the fact that the trace of a positive semidefinite matrix is greater than its spectral value

$$\begin{aligned} &|[A_o d_m(t) \cdots A_r d_m(t)]|^2 \\ &\quad \leqslant \sum_{i=0}^{r} |A_i d_m(t)|^2 \leqslant |d_m(t)|^2 \sum_{i=0}^{r} |A_i|^2. \end{aligned}$$

This argument, along with the time-invariance of A_i, $i \in \{0, \ldots, r\}$, and the definition $\bar{\sigma}^2(\{A_i\}) := \sum_{i=0}^{r} |A_i|^2$ provides

$$\|F(\chi) d_m\|^2 \leqslant (1 + \bar{\chi}^2) \|d_m\|^2 \bar{\sigma}^2(\{A_i\})$$

and ultimately leads to the disturbance attenuation relation

$$\begin{aligned} \|\chi - \hat{\chi}\|^2_{Q(y,v)} \leqslant \gamma^2 \{&2\|d_p\|^2 + \|d_\chi\|^2 + |x_o - \hat{x}_o|^2_{P_o} \\ &+ |\chi_o - \hat{\chi}_o|^2_{Q_o} + [1 + 2\bar{\sigma}^2(\{A_i\})]\|d_m\|^2 \\ &+ 2\bar{\sigma}^2(\{A_i\})\bar{\chi}^2 \|d_m\|^2\}. \end{aligned} \tag{27}$$

The relation in (27) represents meaningful disturbance attenuation in the sense described above, albeit with the unusual term involving the cross product $\bar{\chi}^2 \|d_m\|^2$. The bound $\bar{\chi}$ poses a theoretical difficulty in general since it depends upon $d_\chi(t)$, χ_o, and the nature of the evolution of $\chi(t)$ as captured by H and K. Difficulties would occur if $\chi(t)$ increased without bound due to instability of H or due to a particularly poor choice of $d_\chi(t)$. Such behavior may make the estimate error extremely sensitive to measurement noise. However in the icing case such a bound $\bar{\chi}$ will always exist since there exists more specific information about the evolution of $\chi(t)$ than is available in (10). Hence, high sensitivity to measurement noise would not occur in the present context.

4. Simulation results

Simulations of the H^∞ NPFSI parameter ID algorithm were performed in order to evaluate the accuracy and timeliness of the icing indication. The two icing scenarios depicted in Fig. 1 are considered. In each scenario, excitation is provided only by turbulence. Both iced-aircraft and clean-aircraft simulations were performed. The iced-aircraft simulations investigate a correct indication of icing, whereas the clean-aircraft simulations investigate an incorrect icing indication, or false alarm. In the iced case, the question is whether the parameter estimates can track the actual parameters in a timely fashion. The accuracy of the iced-aircraft estimates must be considered in light of the clean-aircraft estimate error.

The unknown exogenous signals d_m and d_p are determined from a sensor noise model and a turbulence model, respectively. It is assumed that both d_p and d_m are zero-mean, bandlimited white Gaussian noise, with a bandlimit of 10 Hz. Furthermore, both the measurement noise and process noise are assumed to have

Table 2
Measurement noise intensities taken from NASA Twin Otter instrument resolution specifications as reported by Ratvasky and Ranaudo (1993)

σ_q	σ_θ	σ_α	σ_u
0.0167°/s	0.0293°	0.003°	0.039 m/s

uncorrelated elements, and hence are completely characterized by their covariance matrix diagonals. For the measurement noise, these intensities are the NASA Twin Otter instrument resolution specifications as reported by Ratvasky and Ranaudo (1993), and are given in Table 2. The process noise is assumed to be turbulence, which is modeled as independent vertical and horizontal acceleration perturbations (Roskam, 1982). Since the vertical velocity is represented in the state x by α according to $w = U_o\alpha$, turbulence enters the dynamics through α as well as u. A noise intensity corresponding to $0.2g$ of acceleration was used for both α and u, and all other elements of d_p are assumed to be zero.

The algorithm simulated used $Q = \Sigma_2^{\mathrm{T}}\Sigma_1^{-2}\Sigma_2$ so that $\gamma^* \leqslant 1$. A value of γ slightly larger than 1 was chosen, in this case $\gamma = 1.01$, since $\gamma = \gamma^*$ often results in a numerically sensitive algorithm. Some experimentation was used to determine that $Q_o = (1 \times 10^{-5})I$ and $P_o = I$ provided a good combination of noise sensitivity and convergence for the assumed noise. Finally, the simulations included low-pass filtering of the estimated parameters that was implemented as a sliding batch average over the past 15 s. The low-pass filtering is justified since the icing severity is expected to vary on the scale of minutes.

Simulation results for the clean aircraft are shown in Fig. 2, which contains parameter estimates for 25 simulations, each with different turbulence and measurement noise realizations. Although the estimate of M_α varies significantly, its variation does not exceed that consistent with an icing severity of $\bar{\eta} = 0.25$. Hence any estimated parameter variations for M_α beyond this level can be considered an unambiguous icing indication. The simulation results for the moderate icing encounter are given in Fig. 3. The associated tracking delays for various icing severity levels are characterized in Table 3. The important feature of these delays, as can be discerned from Fig. 3, is that the pilot is aware of each icing severity level before the next severity level is actually reached. Finally, the simulation results for the severe icing encounter are given in Fig. 4 and Table 4. In this case, the delay is more substantial in that the pilot does not receive notification for a particular icing severity level before the next level is reached. However, even in this most extreme case, the pilot will receive an unambiguous indication before the icing becomes severe. Put more precisely, the M_α estimate generally

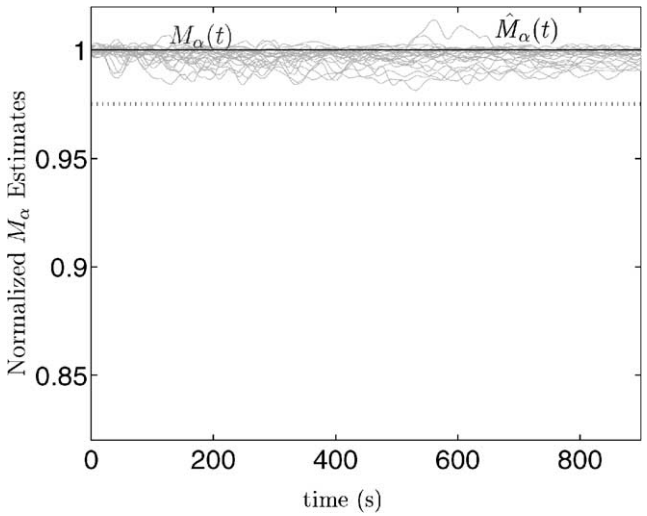

Fig. 2. H^∞ NPFSI identification of M_α for clean aircraft. The dotted line is M_α for $\bar{\eta} = 0.25$.

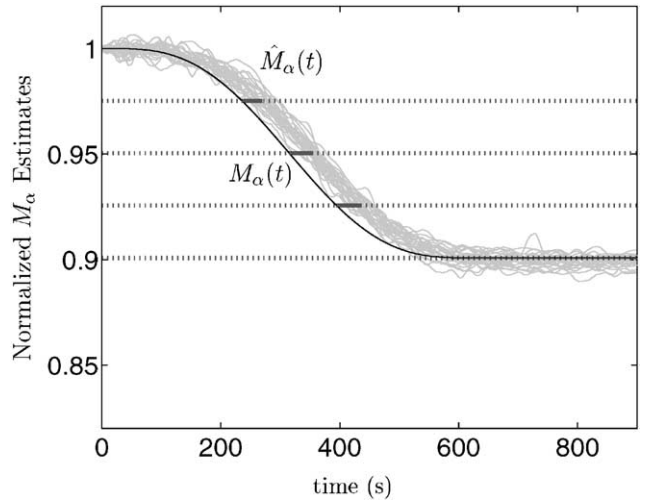

Fig. 3. H^∞ NPFSI identification results for the moderate icing case. The dotted lines represent $\bar{\eta} = 0.25$ increments. The short thick line segments represent the mean delay for each η increment.

Table 3
Icing classification delay statistics for the moderate icing case

	Ice accretion level		
	$\bar{\eta} = 0.25$	$\bar{\eta} = 0.5$	$\bar{\eta} = 0.75$
Mean delay	33.7 s	39.0 s	42.1 s
Delay s.d.	14.7 s	11.6 s	13.7 s

goes below the $\bar{\eta} = 0.25$ value before $\bar{\eta}$ reaches one. This should be sufficient, since there is little danger of inducing a handling event without pilot input for $\bar{\eta} < 1$. If the pilot makes a maneuver during this period, then the previous analysis of Melody et al. (2000) applies, and an icing indication would be available in a matter of seconds.

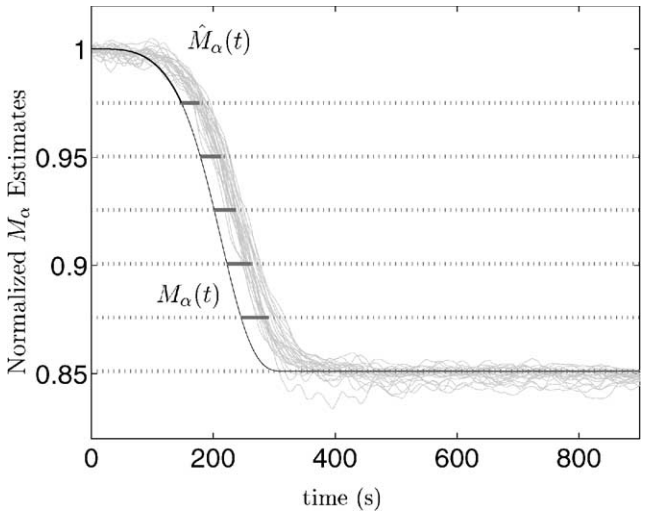

Fig. 4. H^∞ NPFSI identification results for severe icing. The dotted lines represent $\bar{\eta} = 0.25$ increments. The short thick line segments represent the mean delay for each η increment.

Table 4
Icing classification delay statistics for the severe icing case

	Ice accretion level				
	$\bar{\eta} = 0.25$	$\bar{\eta} = 0.5$	$\bar{\eta} = 0.75$	$\bar{\eta} = 1$	$\bar{\eta} = 1.25$
Mean delay	29.9 s	33.8 s	35.6 s	39.1 s	44.9 s
Delay s.d.	7.9 s	8.4 s	8.5 s	8.7 s	12.3 s

It may seem curious that a completely unknown exogenous signal which on the one hand produces parameter estimate error, can on the other hand provide excitation that results in parameter convergence. This fact is the benefit of the state-space formulation of the problem, namely that the state-space formulation, as opposed to a frequency-domain input–output formulation, explicitly contains the effect of the history of the state on the present value of the state. Speaking theoretically, this is in fact the definition of the state, namely, all information about the history of the system pertinent to the future evolution of the system. At any time instant, the unknown present value of the turbulence is a source of error. However, past turbulence has caused the state to move about, and the effect of this past state excitation on the present value of the state is a function of the parameter, χ. Hence measurements, or in this case estimates, of the state provide a means of identifying the parameters. In the case of flight dynamics, this effect is elucidated by (3) which contains M_α. Assuming for the sake of explanation that the state is measured, α and u on the right-hand side of (3) can be thought of as input to the system represented by (3) alone. Turbulence directly affects only α and u, so if the state is measured perfectly, the turbulence provides input excitation to the system of (3) alone in a manner similar to δ_E. In the NPFSI case, the state is not measured perfectly and a state estimate is used in place of the measured state. Even so, the qualitative argument above still applies.

5. Conclusion

This study has investigated the performance of an H^∞ NPFSI ID algorithm in the context of icing detection during steady, level flight with turbulence. As opposed to previously reported results for identification during a maneuver, this study explicitly considers the time-varying nature of the problem. Ice accretion was modeled as a continuous process, where the tailplane icing severity was captured by a severity factor, $\bar{\eta}$. The relation between aircraft stability and control derivatives and the icing severity factor was determined by linearly interpolating between iced and clean aircraft models based on the NASA Twin Otter inflight icing research aircraft. The typical linearization about a trim condition was used, and only longitudinal dynamics were considered. Simulations for the iced and clean aircraft were performed in order to investigate both accurate icing indications and false alarms. The simulation results demonstrate that for both moderate and severe icing encounters, reliable indications of non-negligible levels of icing severity are available prior to the onset of severe icing. These promising results justify further evaluation of the algorithms with the full nonlinear flight dynamics. Ultimately the parameter identification algorithms and ice detection may be coupled with control adaptation, which is left as a future direction of research.

Acknowledgements

This work was supported in part by NASA and in part by the University of Illinois at Urbana-Champaign under the Critical Research Initiatives Program.

References

Bragg, M. B. (1996). Aircraft aerodynamic effects due to large droplet ice accretions. *Proceedings of the 34th AIAA aerospace sciences meeting and exhibit*, number AIAA-96-0932, Reno, NV.

Bragg, M. B., Hutchison, T., Oltman, R., Pokhariyal, D., & Merret, J. (2000). Effect of ice accretion on aircraft flight dynamics. *Proceedings of the 38th AIAA aerospace sciences meeting and exhibit*, number AIAA-2000-0360, Reno, NV.

Bragg, M. B., Perkins, W. R., Sarter, N. B., Başar, T., Voulgaris, P. G., Gurbacki, H. M., Melody, J. W., & McCray, S. A. (1998). An interdisciplinary approach to inflight aircraft icing safety. *Proceedings of the 36th AIAA aerospace sciences meeting and exhibit*, number AIAA-98-0095, Reno, NV.

Cole, J., & Sands, W. (1991). Statistical study of aircraft icing accidents. *Proceedings of the 29th AIAA aerospace sciences meeting and exhibit*, number AIAA-91-0558, Reno, NV.

Didinsky, G., Pan, Z., & Başar, T. (1995). Parameter identification of uncertain plants using H^{∞} methods. *Automatica*, *31*(9), 1227–1250.

Khalil, H. K. (1996). *Nonlinear systems* (2nd ed.). Upper Saddle River, NJ: Prentice-Hall.

Melody, J. W., Basar, T., Perkins, W. R., & Voulgaris, P. G. (2000). Parameter identification for inflight detection of aircraft icing. *Control Engineering Practice*, *8*(9), 985–1001.

Melody, J. W., Pokhariyal, D., Merret, J., Başar, T., Perkins, W. R., & Bragg, M. B. (2001). Sensor integration for inflight icing characterization using neural networks. *Proceedings of the 39th AIAA aerospace sciences meeting and exhibit*, number AIAA-2001-0542, Reno, NV.

NAS, (1997). Weather investment recommendations, *Technical report*, NASA Aeronautics Safety Investment Strategy.

Ratvasky, T. P., & Ranaudo, R. J. (1993). Icing effects on aircraft stability and control determined from flight data. *Proceedings of the 31st AIAA aerospace sciences meeting and exhibit*, number AIAA-93-0398, Reno, NV.

Ratvasky, T. P., Van Zante, J. F., & Riley, J. T. (1999). NASA/FAA tailplane icing program overview. *Proceedings of the 37th AIAA aerospace sciences meeting and exhibit*, number AIAA-99-0370, Reno, NV.

Roskam, J. (1982). *Airplane flight dynamics and automatic flight controls* (2nd ed.). Ottawa, KS: Roskam Aviation and Engineering Corporation.

Schuchard, E. A., Melody, J. W., Başar, T., Perkins, W. R., & Voulgaris, P. (2000). Detection and classification of aircraft icing using neural networks. *Proceedings of the 38th AIAA aerospace sciences meeting and exhibit*, number AIAA-2000-0361, Reno, NV.